ISSN 1674-1056
http://cpb.iphy.ac.cn
http://iopscience.iop.org/cpb
中国物理 B
Chinese Physics
中国物理 Chinese Physics B

First principles study on lattice vibration and electrical properties of layered perovskite $Sr_2M_2O_7$(M=Nb, Ta)

Xing Liu(刘星), Hui-Qing Fan(樊慧庆)

Citation: Chin. Phys. B . 2018, 27(8): 086104. **doi:** 10.1088/1674-1056/27/8/086104

Journal homepage: http://cpb.iphy.ac.cn; http://iopscience.iop.org/cpb

What follows is a list of articles you may be interested in

First-principles study of the $(Cu_xNi_{1-x})_3Sn$ precipitations with different structures in Cu-Ni-Sn alloys

Guang-Wei Peng(彭广威), Xue-Ping Gan(甘雪萍), Zhou Li(李周), Ke-Chao Zhou(周科朝)
Chin. Phys. B . 2018, 27(8): 086302. **doi:** 10.1088/1674-1056/27/8/086302

First principles study of ceramic materials (IVB group carbides) under ultrafast laser irradiation

Nan-Lin He(何南燐), Xin-Lu Cheng(程新路), Hong Zhang(张红), Gai-Qin Yan(闫改琴), Jia Zhang(张佳)
Chin. Phys. B . 2018, 27(3): 036301. **doi:** 10.1088/1674-1056/27/3/036301

Simulations of guiding of low-energy ions through a single nanocapillary in insulating materials

Shi-Dong Liu(刘世东), Yong-Tao Zhao(赵永涛), Yu-Yu Wang(王瑜玉)
Chin. Phys. B . 2017, 26(10): 106104. **doi:** 10.1088/1674-1056/26/10/106104

Channeling of fast ions through the bent carbon nanotubes: The extended two-fluid hydrodynamic model

Lazar Karbunar, Duško Borka, Ivan Radović, Zoran L Mišković
Chin. Phys. B . 2016, 25(4): 046106. **doi:** 10.1088/1674-1056/25/4/046106

Analytical model for describing ion guiding through capillaries in insulating polymers

Liu Shi-Dong, Zhao Yong-Tao, Wang Yu-Yu, Stolterfoht N, Cheng Rui, Zhou Xian-Ming, Xu Hu-Shan, Xiao Guo-Qing
Chin. Phys. B . 2015, 24(8): 086104. **doi:** 10.1088/1674-1056/24/8/086104

First principles study on lattice vibration and electrical properties of layered perovskite $Sr_2M_2O_7$ (M = Nb, Ta)*

Xing Liu(刘星)† and Hui-Qing Fan(樊慧庆)‡

State Key Laboratory of Solidification Processing, School of Materials Science and Engineering, Northwestern Polytechnical University, Xi'an 710072, China

(Received 27 December 2017; revised manuscript received 4 May 2018; published online 10 July 2018)

In this paper, we performed calculations to investigate the dielectric, piezoelectric properties, Born effective charge (BEC), and spontaneous polarization of $Sr_2M_2O_7$, the method used in our study was a well-known density functional theory based on first-principles. The optimized results were in good agreement with previous experiments and calculations, which indicates that our calculated method is reasonable. The research we have done suggested that greater piezoelectric components of $Sr_2Nb_2O_7$ were e_{31} and e_{33}, and the contributions were derived from the A_1. By studying the Born effective charge, it could be seen that the valence of ions changed, and the O of $Sr_2Nb_2O_7$ were most obviously that caused by the covalent character of ions and the hybridization of O-2p and Nb-4d. The spontaneous polarization of $Sr_2Nb_2O_7$ in the [001] direction is 25 μC/cm^2, while for $Sr_2Ta_2O_7$, there was no spontaneous polarization in the paraelectric state. Finally, the effect of pressure on the piezoelectric properties were also investigated, the polarization of $Sr_2Nb_2O_7$ decreased linearly with the increase after pressure. All our preliminary results throw light on the nature of dielectric, piezoelectric properties, Born effective charge, and spontaneous polarization of $Sr_2M_2O_7$, it was helpful for experimental research, the development of new materials, and future applications.

Keywords: $Sr_2M_2O_7$, first-principles, dielectric and piezoelectric properties, Born effective charge, spontaneous polarization

PACS: 63.20.dk, 71.15.Mb, 77.90.+k **DOI:** 10.1088/1674-1056/27/8/086104

1. Introduction

Layered perovskite structure $Sr_2M_2O_7$, as a new type of functional material, has become a hot topic,[1–4] for instance, Cai *et al.* studied the dielectric constant and loss of $Sr_2Nb_2O_7$ specimen sintered at 1200 °C, which were 57% and 1.6% at 10 kHz, and the piezoelectric constant d_{33} reached 2.1 pC/N, respectively. In Chen's work, by using the solid-state reaction method, the author investigated significant effects on the sinterability, microstructure, and electrical properties of $Sr_2Nb_2O_7$ ceramics prepared by CuO addition. Peng *et al.* studied the electronic structures of S and V/Nb mono- and (anionic–cationic) co-doped $Sr_2Ta_2O_7$, the band gap engineering and the shifts of the VBM and CBM for sufficiently utilizing visible light of the solar spectrum by generalized gradient approximation (GGA) and Perdew–Burke–Eruzerh (PBE) calculations. Teshima *et al.* prepared $Sr_2Ta_2O_7$ film growth under several different conditions, and found that the growth atmospheres were important in forming idiomorphic crystals with well-developed facets and characteristic shapes. The above results provide a comparison and research direction for our theoretical calculation.

At room temperature, $Sr_2Nb_2O_7$ and $Sr_2Ta_2O_7$ are orthogonal structures (see Fig. 1), which are composed of many "plates" that are parallel to (010) planes (seen Fig. 1), and every "plate" is composed of the MO_6 octahedrons. One of Sr occupies the boundary of the structure, another Sr in internal system, for M, there are also two types and all locate at the center of the octahedron. $Sr_2Ta_2O_7$ (space group *Cmcm*) and $Sr_2Nb_2O_7$ (space group $Cmc2_1$) are isomorphic heterogeneity, the symmetry of $Sr_2Ta_2O_7$ is higher than that of $Sr_2Nb_2O_7$ at room temperature.

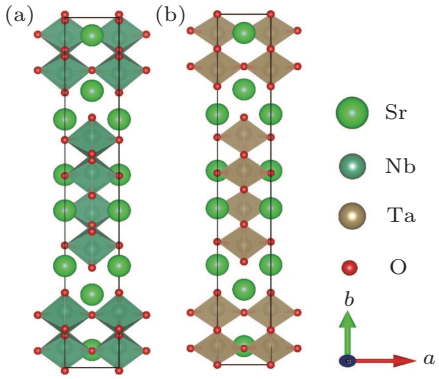


Fig. 1. (color online) The perovskite-slab structures of $Sr_2M_2O_7$ unit cell, the green and brown regions represent NbO_6 and TaO_6 octahedra, respectively.

Because of the unique structure and excellent physical properties, $Sr_2M_2O_7$ can also be widely used in various in-

*Project supported by the National Natural Science Foundation of China (Grant No. 51672220), the 111 Program of the Ministry of Education of China (Grant No. B08040), the National Defense Science Foundation (Grant No. 32102060303), the Xi'an Science and Technology Foundation, the Shaanxi Provincial Science Foundation and the Gaofeng Project of Northwestern Polytechnical University, China (Grant No. 17GH020824).

†Corresponding author. E-mail: xingliu_lx@163.com

‡Corresponding author. E-mail: hqfan3@163.com

© 2018 Chinese Physical Society and IOP Publishing Ltd

dustrial fields. For $Sr_2Nb_2O_7$, it is one of the few high temperature ferroelectric materials with high Curie temperature (T_c = 1615 K), chemical and thermal stability, and significant physical properties.[5,6] As a new photocatalyst, $Sr_2Ta_2O_7$ is the paraelectric orthorhombic phase at room temperature without any additives to split water into H_2 and O under UV light.[7] The unique structure determines that $Sr_2M_2O_7$ has many advantages: (i) it is easy to adjust the band gap and absorption spectrum of the semiconductor by changing the particle size; (ii) the optical absorption of semiconductor particles present absorption bands, which is beneficial to the effective collection of sunlight; (iii) the photostability can be increased by the surface modification; (iv) using layers as a suitable reaction point to control the reverse reaction, the efficiency of the reaction can be improved, therefore, the semiconductors that enter layers are in the nanometer scale, it is beneficial to the separation of photogenerated electrons and holes; (v) when the semiconductor is irradiated by the light, it can generate the conduction electron and the corresponding hole. The excited state of electrons can recombine with the holes, and the light energy can be converted into thermal energy or other forms of energy in the process of recombinations. After the combination of semiconductors and layered compounds, there are effective migrations of photoelectrons from semiconductors to layered substrates, and the generated electron–hole pairs in the semiconductor surface cannot be quickly combined for other reasons; the semiconductor has activity, showing that the reason for the inhibition of electron–hole pairs recombination may be that the semiconductors are affected. In this case, electron–hole pairs recombination will be significantly suppressed, which also reduces the recombination rate of photogenerated electrons and holes, thereby improving the photocatalytic properties of semiconductor. On the side, due to the special layered structure, the metal, non-metal, organics, semiconductor oxide, and composite nanoparticles can be introduced into the interlayers, to improve the thermal stability and catalytic activity, because of the great concern.[4,8]

Since Nanamatsu *et al.*[9] first successfully synthesized $Sr_2Nb_2O_7$, $Sr_2Ta_2O_7$, and the corresponding solid solution by the floating zone method, several researchers have experimentally and theoretically investigated related properties of $Sr_2M_2O_7$. Kudo *et al.*[10] studied the perovskite-tantalates $Sr_2(Ta_{1-x}Nb_x)_2O_7$, band structure, and water splitting activity by partial substitution of Nb; the results indicated that the band gap decreases with the increase of Nb/Ta. After loading the NiO, the photolysis of water according to the stoichiometric produced H_2 and O, NiO/$Sr_2Ta_2O_7$ had the highest activity. Kato *et al.*[11] researched the surface morphology and dielectric properties of $Sr_2Ta_2O_7$ and $Sr_2(Ta_{0.7}Nb_{0.3})_2O_7$ films when the annealing temperature reached 750 °C, the dielectric constant was around 90, while dielectric loss was less than 0.05 at 100 kHz, which showed that these compounds were suitable for memory materials. Yoshioka *et al.*[12] investigated the relationship between photocatalytic activity and crystal structure of different perovskite tantalate ($Sr_2Ta_2O_7$, $Sr_2Ta_2O_6$, and $Sr_4Ta_2O_9$). The research suggested that $Sr_2Ta_2O_7$ had the highest photocatalytic and great relationship with special structure. TaO_6 octahedrons in $Sr_2Ta_2O_7$ were connected with the common vertex, while the common surface for the TaO_6 in $Sr_4Ta_2O_9$. Thus, the conduction bands of $Sr_4Ta_2O_9$ were so narrow that it cannot provide effective carrier and the poor photocatalytic activity.

With the development of computers, the theoretical researches of materials have increased, especially based on the first principles.[13–15] Nisar *et al.*,[16] based on hybrid functionals (HSE06), surveyed the photocatalytic of $Sr_2Nb_2O_7$ from the band structure and bandgap. The results showed that the band gap in layered perovskite $Sr_2Nb_2O_7$ was significantly reduced by the cationic–anionic co-doping, and band position was excellent for the visible-light photocatalysis. Liu *et al.*[17] performed hybrid functional calculations for the mono- and co-doping of $Sr_2Ta_2O_7$ by the controlled band gap engineering for an efficient solar-driven photocatalyst. The results showed that doping creates impurity states in the band gap and therefore reduces the band gap significantly, and the stability of the co-doped system is governed by the Coulomb interactions and charge compensation effects.

By reviewing the previous work, we find that the researches about $Sr_2M_2O_7$ have made great achievements both in experiment and theory, but these studies mainly focused on optical research under UV light and there have been few theoretical calculations that were not systematic. The present study, based on first-principles, will focus on the discussion of dielectric, piezoelectric properties, Born effective charge, and spontaneous polarization of $Sr_2M_2O_7$. As is known to all, the above properties have been widely applied in the field of photoelectricity, especially photocatalytic degradation of organic pollutants, photolysis of water to produce ammonia. More and more attention has been paid to the degradation of environmental pollutants and the decomposition of water by using solar semiconductor photocatalysis technology. It is expected to solve the problems of energy shortage and environmental pollution, therefore our preliminary research can provide important theoretical guidance for studying $Sr_2M_2O_7$ and expanding its application.

2. Computational details

Because many experiments are difficult or costly in practice, the theoretical calculation is usually the first step in this experiment. Piezoelectricity is one of the most important practical properties of ferroelectric materials, so the theoretical investigation of dielectric and piezoelectric properties is taken as the first step to guide the practice.

We used the generalized gradient approximation (GGA)[12] in the Perdew–Burke–Eruzerh (PBE)[18] to study $Sr_2M_2O_7$, and the theoretical mechanisms are discussed. The calculations have been performed by using the Cambridge Sequential Total Energy Package (CASTEP) code.[19,20] Using the plane wave pseudopotential method, the ion potential is replaced and the electron wave function is carried out with the plane wave basis set. We use the GGA to correct the exchange interaction between the electrons and the correlation potential.

In the density functional theory (DFT), the Schrödinger equation of the single electron motion can be expressed as follows (in atomic unit):

$$\left[-\frac{\nabla^2}{2}-\sum_q \frac{Z_q}{|r-R_q|}+\int \frac{\rho(r)}{|r-r'|}\mathrm{d}r'+V(r)\right]\Psi_i(r)=\varepsilon_i\Psi_i(r), \tag{1}$$

$$\rho(r)=\sum_i^{n_i}|\Psi_i(r)|^2, \tag{2}$$

where Z_q is the nuclear charge, r is the position vector of the nuclear motion, R_q is the distance between two cores, $\rho(r)$ indicates the electron density, $V(r)$ indicates the external potential field, $\Psi_i(r)$ is a single electron wave function, ε_i is the energy of a single electron, and n_i indicates the number of electrons occupied by the intrinsic state. The first term is effective electron kinetic energy in the system of Eq. (1). The second represents the attractive Coulomb potential of the atoms in the system, which is expressed by the norm-conserving pseudopotential. The term is electron Coulomb potential. The fourth represents the exchange correlation energy, and the concrete form is expressed by the local density approximation (LDA) or the GGA.

The valence electron configuration for Sr, Nb, Ta, and O are $4p^65s^2$, $4d^65s^1$, $5p^65d^3$, and $2s^22p^4$, respectively. The ultrasoft pseudopotential is applied to describing the interaction energy between valence electron and ionic core. The Brillouin zone integration is performed over $4\times4\times8$ grid sizes using the Monkhorst–Pack method for structure optimization. The convergence thresholds for total energy, maximum force, maximum stress, maximum displacement, and Hellmann–Feynman ionic force are less than 5×10^{-6} eV/atom, 0. 01 eV/Å, 0. 02 GPa, 5.0×10^{-4} Å, and 1 meV/Å. The linear response method of density functional perturbation theory (DFPT)[21] is used to calculate the dielectric, piezoelectric properties, Born effective charge, and the calculation of spontaneous polarization using the Berry phase method.[22]

3. Results and discussion

From Table 1, it can be seen that the optimized structures are consistent with the experimental data,[16,23] indicating that our calculations are reasonable. Nisar *et al.*[16] simulated the structures of $Sr_2Nb_2O_7$ and $Sr_2Ta_2O_7$ using hybrid functionals and PBE function. The result shows that the error rate is greater than 1.2% for $Sr_2Nb_2O_7$, and greater than 1.6% for $Sr_2Ta_2O_7$. The PBE usually overestimates the lattice parameters of the equilibrium, so the PBEsol function is more suitable for our work.

Table 1. The space groups and lattice parameters (in unit Å) of the $Sr_2Nb_2O_7$ and $Sr_2Ta_2O_7$.

$Sr_2Nb_2O_7$				$Sr_2Ta_2O_7$			
$Cmc2_1$	Present	HSE06[16]	Expt.[22]	$Cmcm$	Present	PBE[23]	Expt.[22]
a/Å	3.9820	3.797	3.97	a/Å	3.9572	3.983	3.95
b/Å	26.9472	27.205	26.86	b/Å	27.3434	27.59	27.27
c/Å	5.7239	5.793	5.72	c/Å	5.6969	5.746	5.70

3.1. Lattice vibrations of Γ points for $Sr_2M_2O_7$

$Sr_2Nb_2O_7$ has 4 different phonon modes (A_1, A_2, B_1, and B_2), which are one-fold degeneracy. Phonon frequencies at the center (Γ) of the Brillouin zone are listed in Table 2. Based on the group theory, the irreducible representation of $Sr_2Nb_2O_7$ phonon modes is expressed as follows:

$$\Gamma=21A_1\oplus11A_2\oplus10B_1\oplus21B_2.$$

In order to get the stability configuration of the local potential energy in the lowest point, we must ensure that no imaginary frequency appears. We further calculated the phonon dispersion of $Sr_2M_2O_7$, it can be seen that an imaginary frequency cannot be found from Fig. 2, which indicates that the $Sr_2M_2O_7$ structures are stable.

In terms of optical activity, except for the A_2, the other modes are both infrared and Raman. According to the Mulliken symbol, A_1 and A_2 for the main axis are symmetric, while B_1 and B_2 are antisymmetric. On the other hand, A_1 and B_1 are symmetric for twofold C_2 (perpendicular to the main axis), while A_2 and B_2 are antisymmetric for C_2. In addition, the

phonon at the Γ does not have an imaginary frequency indicating that the optimized structure is stable. In the experiment, Ito *et al.*[19] used Raman scattering and far-infrared scattering to study the phonon frequency of $Sr_2Nb_2O_7$. Because of the experimental conditions, they just observed eighteen A_1, six A_2, five B_1, and two B_2, which are less than expected. Compared with the experiment, the calculated A_1 frequencies are in good agreement with Ito's results. The observed modes in the experiment are less than the calculation, which may be the reason why the unobserved oscillators are relatively weak.

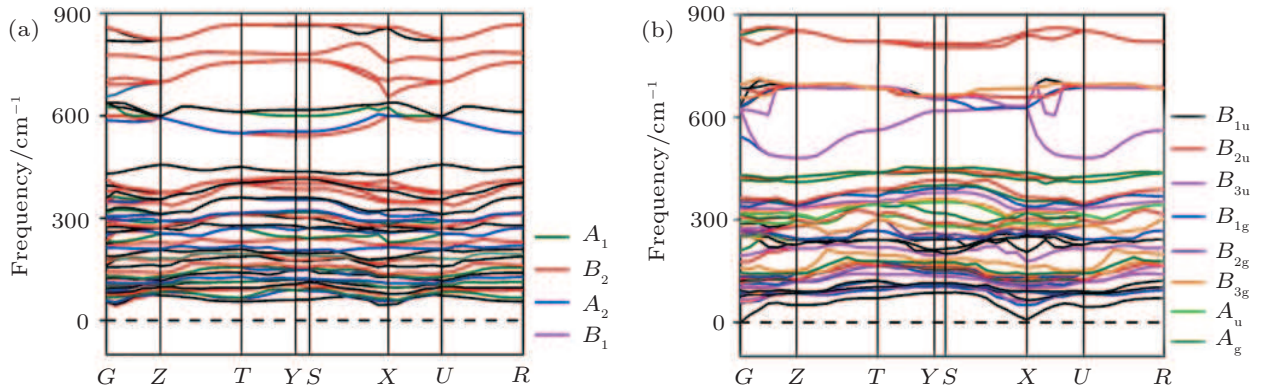


Fig. 2. (color online) The phonon dispersion curves for $Sr_2M_2O_7$, (a) $Sr_2Nb_2O_7$ and (b) $Sr_2Ta_2O_7$, different color curves represent different phonon modes, respectively.

Table 2. Calculated frequencies (in unit cm^{-1}) of phonon modes at the Γ point of $Sr_2Nb_2O_7$.

Irrep	ω_λ/(cm^{-1})		Irrep	ω_λ/(cm^{-1})	
	Present	Previous[22]		Present	Previous[22]
	838.5	850		839.5	834
	820.6	848		783.8	776
	665.7	673		699.7	
	605.2	599		669.5	
	572.2	585		554.1	
	428.1	460		511.5	
	398.5	427		412.4	
	359.1	376		378.8	
	322.2	342		353.5	
	306.5	329		345.6	
	275.8	281		289.1	
A_1	259.7		B_2	279.9	
(IR & Raman)	225.3	242	(IR & Raman)	234.6	
	191.8			223.1	
	161.7	162		185.1	
	156.1	151		170.7	
	129.8	124		141.7	
	124.1	124		123.7	
	93.1	99		107.2	
	81.5			76.1	
	55.5	59		55.3	
	542.3	541		564.9	
	510.6			511.5	
	352.3	340		355.8	342
	310.2			315.2	
A_2	295.5		B_1	288.0	285
(Raman)	250.1		(IR & Raman)	234.6	258
	210.9	220		178.1	179
	130.1	132		130.5	120
	111.4	115		100.7	
	90.9			67.9	
	58.6	60			

For $Sr_2Ta_2O_7$, there are 8 different phonon modes (A_g, B_{1g}, B_{2g}, B_{3g}, A_u, B_{1u}, B_{2u}, and B_{3u}), and all modes are also onefold degeneracy. The irreducible representation at the Γ is expressed as:

$$\Gamma = 10A_g \oplus 8B_{1g} \oplus 10B_{3g} \oplus 2B_{2g} \oplus 3A_u \oplus 11B_{1u} \oplus 8B_{3u} \oplus 11B_{2u}.$$

Table 3. Calculated frequencies (in unit of cm^{-1}) of IR modes at the Γ of $Sr_2Ta_2O_7$.

Irrep	ω_λ/cm^{-1}	Irrep	ω_λ/cm^{-1}	Irrep	ω_λ/cm^{-1}
	676.8		863.9		612.6
	609.3		800.2	561.3	
	575.3		625.7		332.4
	291.4		422.4		273.0
	233.4		423.3		193.9
B_{1u}	222.1	B_{2u}	357.7	B_{3u}	114.0
	201.1		308.9		102.0
	121.9		243.1		66.3
	92.2		179.9		
	73.8		127.2		
	0.56		115.6		

Table 4. Calculated frequencies (in unit of cm^{-1}) of Raman and static modes at the Γ of $Sr_2Ta_2O_7$.

Irrep	ω_λ/cm^{-1}	Irrep	ω_λ/cm^{-1}	Irrep	ω_λ/cm^{-1}
	856.7		593.0		695.9
	812.0		560.8		624.9
	424.1		342.7		324.5
	411.3		240.3		286.6
A_g	347.4	B_{1g}	137.1	B_{3g}	235.2
(Raman)	315.0	(Raman)	112.9	(Raman)	202.1
	197.6		84.3		159.2
	143.4		57.7		142.4
	119.1				88.7
	101.6				60.6
	321.6		343.0		
A_u	300.6	B_{2g}	266.9		
(Static)	232.4	(Raman)			

From the point of view of optical activity, B_{1g}, B_{3g}, and A_u are Raman activity, while B_{1u}, B_{2u}, and B_{3u} are infrared, the remaining A_g is static. According to the Mulliken symbol, A_g and A_u for the main axis are symmetric, the others, namely B_{1g}, B_{2g}, B_{3g}, B_{1u}, B_{2u}, and B_{3u}, are antisymmetric. On the other hand, A_g, B_{1g}, B_{2g}, and B_{3g} are symmetric for the inversion center, while A_u, B_{2u}, and B_{3u} are antisymmetric. In addition, different from $Sr_2Nb_2O_7$, $Sr_2Ta_2O_7$ has an imaginary frequency (infrared B_{1u} mode, -0.56 cm^{-1}) at the Γ point. The infrared frequencies at the center Γ of the Brillouin zone are listed in Table 3, and the Raman and static frequencies are shown in Table 4. Unfortunately, there is no experimental data to compare.

In the present work, we investigated the atom displacement, in order to better understand the lattice vibration. The M2 atoms are located at the center of the orthogonal $Sr_2M_2O_7$ as shown in Fig. 3. Therefore, with the orderly rotation of the octahedron, the atomic displacement of M2 are always 0. The M1 atoms are symmetrically distributed in the body center of the MO_6 octahedron in the orthogonal $Sr_2M_2O_7$, and clockwise rotation occurs with the rotation of the central axis. All the O atoms on the octahedron move orderly with the rotation of the M1 atom.

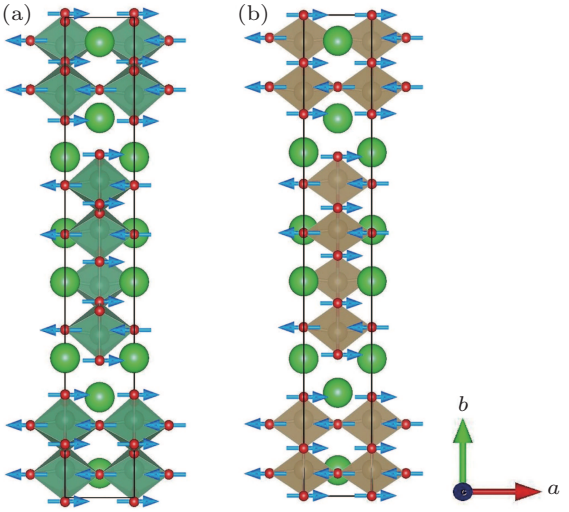


Fig. 3. (color online) The atomic displacement for $Sr_2M_2O_7$, (a) $Sr_2Nb_2O_7$ and (b) $Sr_2Ta_2O_7$, the blue arrows represent the vibration direction of atom O.

3.2. $Sr_2M_2O_7$ electrical properties

The dielectric constants, contributions of electrons and phonons to the dielectric constants, are shown in table 5. According to the symmetry, the dielectric constant for an orthogonal structure has three independent components: ε_{11}, ε_{22}, and ε_{33}, the expression is as follows:

$$\overline{\varepsilon} = \frac{1}{3}\sum_{\alpha=1}^{3}\varepsilon_{ij}. \quad (3)$$

The contributions of electrons to dielectric constants from $Sr_2Nb_2O_7$ are between 4.6–5.2, and the average $\overline{\varepsilon}_\infty$ is 4.9. The total dielectric constants are $\varepsilon_{11} = 65.8$, $\varepsilon_{22} = 31.4$, and $\varepsilon_{33} = 43$, and the results of the experiment[7] were $\varepsilon_{11} = 75$, $\varepsilon_{22} = 46$, and $\varepsilon_{33} = 43$. Obviously, ε_{33} is very approximate to the experimental value, while ε_{11} and ε_{22} are less than the results in the experiment. The dielectric constants of $Sr_2Ta_2O_7$ were $\varepsilon_{11} = 39.4$, $\varepsilon_{22} = 18.1$, and $\varepsilon_{33} = 74.5$, respectively, while the previous results[7] are $\varepsilon_{11} = 37$, $\varepsilon_{22} = 22$, $\varepsilon_{33} = 644$, because of the limited experimental conditions at that time, it was impossible to determine whether the space group of $Sr_2Ta_2O_7$ was *Pbcn* or *Cmcm*.

Table 5. Calculated electronic ($\varepsilon_{\infty,ij}$) and phonon contributions ($\varepsilon_{\mathrm{ph},ij}$), average dielectric constants ($\overline{\varepsilon}_{\infty,ij}$), and total dielectric constants ($\varepsilon_{ij}=\varepsilon_{\infty,ij}+\varepsilon_{\mathrm{ph},ij}$) for $Sr_2Nb_2O_7$ and $Sr_2Ta_2O_7$.

	$Sr_2Nb_2O_7$						$Sr_2Ta_2O_7$					
		11	22	33				11	22	33		
Cal.	$\varepsilon_{\infty,ij}$	5.2	4.6	5.0	$\overline{\varepsilon}_{\infty,ij}$	4.9	$\varepsilon_{\infty,ij}$	4.6	4.3	4.7	$\overline{\varepsilon}_{\infty,ij}$	4.5
	$\varepsilon_{\mathrm{ph},ij}$	60.6	26.8	38.0	$\overline{\varepsilon}_{\mathrm{ph},ij}$	41.8	$\varepsilon_{\mathrm{ph},ij}$	34.8	13.8	69.8	$\overline{\varepsilon}_{\mathrm{ph},ij}$	39.5
	ε_{ij}	65.8	31.4	43.0	$\overline{\varepsilon}_{ij}$	46.7	ε_{ij}	39.4	18.1	74.5	$\overline{\varepsilon}_{ij}$	44.0
Expt.[5]	ε_{ij}	75	46	43.1	$\overline{\varepsilon}$	54.7	ε_{ij}	37	22	644	$\overline{\varepsilon}$	234.3

The dielectric constants of $Sr_2Nb_2O_7$ are not high, so is the measured dielectric loss in the experiment. However, materials with ferroelectric properties at high temperature can be used for ferroelectric random storage materials.[24] Table 6 lists the phonon frequency and oscillator strength of $Sr_2Nb_2O_7$ with major contributions to the dielectric constant. We can see that greater contributions are the frequency of 124.1, 55.5, 178.1, 100.7, and 55.3 cm^{-1}. Table 7 lists the contribution of ions to dielectric constants in $Sr_2Nb_2O_7$. The main contribution to the dielectric constants are Nb_1 and O_3–O_7 ions, in other words, the covalent structure of NbO_6 is formed by these ions, which contribute greatly to the dielectric constants.

Table 6. The calculated mode frequencies ω_λ (in unit of cm^{-1}), the oscillator strength, make dominant contributions to the dielectric intensity for $Sr_2Nb_2O_7$.

ω_λ (A_1)	$S_{\lambda,33}$	ω_λ (B_1)	$S_{\lambda,11}$	ω_λ (B_2)	$S_{\lambda,22}$
124.1	9.3	178.1	33.4	76.1	4.8
93.1	2.7	100.7	16.4	55.3	9.9
81.5	5.7	67.9	4.6		
55.5	8.4				

Table 7. Contributions of individual ions ($\varepsilon_{k,ij}$) to the dielectric constants for $Sr_2Nb_2O_7$.

Atom	WP	$\varepsilon_{k,11}$	$\varepsilon_{k,22}$	$\varepsilon_{k,33}$
Sr1	4*a*	−0.593	3.711	3.072
Sr2	4*a*	0.011	0.123	0.478
Nb1	4*a*	10.805	−0307	1.649
Nb2	4*a*	0.89	−1.972	3.139
O1	4*a*	1.394	1.695	−0.848
O2	4*a*	0.582	0.665	−0.693
O3	4*a*	3.191	2.835	6.143
O4	4*a*	1.597	1.718	3.175
O5	4*a*	3.847	0.843	1.013
O6	4*a*	6.825	0.982	2.988
O7	4*a*	2.344	3.178	5.147

In order to analyze the origin of the components in the dielectric tensor, the oscillators strength of greater frequencies and the effective charge of different frequencies are shown in Table 8. According to symmetry, the oscillator strength of B_{1u} has a non-zero component $S_{\lambda,33}$, and B_{2u} only contributes to $S_{\lambda,22}$. The major contribution to $S_{\lambda,22}$ is the infrared phonons of 308.9 cm^{-1} and 115.6 cm^{-1}, the oscillator strength is 4.9 and 5.2, and the effective charges are 7.5 and 5.1, respectively. The dielectric component $\varepsilon_{\mathrm{ph},11}$ is mainly contributed by B_{3u} of 193.9 cm^{-1} and 102.9 cm^{-1}, and the $\varepsilon_{\mathrm{ph},33}$ is derived from the B_{1u}, 121.9 cm^{-1} and 92.2 cm^{-1}.

Table 8. The calculated mode frequencies ω_λ (in unit of cm^{-1}), oscillator strength, and mode effective charge (e) make dominant contributions to the dielectric intensity for $Sr_2Ta_2O_7$.

ω_λ	B_{1u}		ω_λ	B_{3u}		ω_λ	B_{2u}	
	$S_{\lambda,33}$	$\lvert Z^*_\lambda\rvert$		$S_{\lambda,11}$	$\lvert Z^*_\lambda\rvert$		$S_{\lambda,22}$	$\lvert Z^*_\lambda\rvert$
121.9	3.4	3.2	193.9	21.0	10.1	308.9	4.9	7.5
92.2	17.1	5.8	102.9	7.66	6.1	115.6	5.2	5.1
73.8	37.3	5.3						

Phonon's contribution to the dielectric constants can be decomposed into the contributions of each ion (Table 9). It can be seen that contributions from O1, O2, and O5 to $\varepsilon_{\mathrm{ph},11}$ is major. The greatest contribution to $\varepsilon_{\mathrm{ph},22}$ is Sr_1 and O_5. The main contribution to $\varepsilon_{\mathrm{ph},33}$ is Sr_2, O1, and O4, and O1 with a value of about 5.596.

Table 9. The contribution ($\varepsilon_{k,ij}$) of ions in $Sr_2Ta_2O_7$ to the phonon dielectric constants.

Atom	WP	$\varepsilon_{k,11}$	$\varepsilon_{k,22}$	$\varepsilon_{k,33}$
Sr1	4*c*	0.683	1.423	1.994
Sr2	4*c*	1.409	0.109	3.433
Ta1	4*c*	2.011	0.366	1.230
Ta2	4*c*	0.419	0.625	1.871
O1	4*c*	4.193	0.516	5.596
O2	4*c*	2.953	0.504	1.426
O3	8*f*	0.893	0.524	0.007
O4	8*f*	1.403	1.132	4.686
O5	4*a*	2.424	1.304	3.243

Orthogonal structure $Sr_2Nb_2O_7$ exhibits the ferroelectric state, and the piezoelectric constant has five independent components (Table 10), of which, the larger values are e_{31} (1.276) and e_{33} (−2.932), respectively, while $Sr_2Ta_2O_7$ has no piezoelectric constant.

Generally known, the piezoelectric strain coefficient can be expressed as,

$$d_{\mathrm{iv}} = \sum_{\mu=1}^{6} e_{\mathrm{iu}} S_{\mu v}, \quad S = \frac{1}{C}, \tag{4}$$

where S represents the elastic compliance constant, and C represents the elastic stiffness constant. The obtained elastic constants from the calculation are $C_{11} = 113.8$ GPa, $C_{22} = 120.1$ GPa, and $C_{33} = 196.8$ GPa, which are in agreement with the existing experimental data.[25] The piezoelectric constant is obtained by further calculation, $d_{33} = 24$ pC/N, while the measured $d_{33} = 2.8$ pC/N in the experiment.[26]

Table 10. Homogeneous strain contribution ($e_{iv,\mathrm{hom}}$) and internal-strain contribution ($e_{iv,\mathrm{int}}$) to the total piezoelectric stress constants element $e_{iv,\mathrm{tot}}$ (in units C/m^2). We use the Voigt notion, the Latin index i runs from 1 to 3, and the Greek index v from 1 to 6.

	e_{15}	e_{24}	e_{31}	e_{32}	e_{33}
$e_{iv,\mathrm{hom}}$	0.212	.081	-0.122	.201	0.110
$e_{iv,\mathrm{int}}$	0.783	0.909	1.398	.602	2.813
$e_{iv,\mathrm{tot}}$	0.995	.990	1.276	.803	2.932

The contributions of different phonon modes to the internal-strain piezoelectric constants in $Sr_2Ta_2O_7$ (Table 11) are further analyzed. Based on symmetry, we can know that the contributions of e_{31} and e_{33} to the piezoelectric components come from the A_1. For e_{31}, it can be seen that the main contribution is A_1 of 81.5 cm^{-1} and 55.5 cm^{-1}, while e_{33}, the contributions come from 124.1 cm^{-1} and 82.5 cm^{-1}. Compared with the phonon contribution to the dielectric, it can be found that the phonon contributions to the piezoelectric and dielectric components are consistent. Dielectric and piezoelectric responses are polarizable properties, which can be expressed as polarization about the applied electric field and macroscopic strain. Both of them can be understood as the contribution of electron and the relative displacement of ionic lattice.

Table 11. Contribution of A_1 to the internal-strain piezoelectric constants $e_{iv,\mathrm{int}}$ (in units C/m^2).

ω_λ	e_{31}	e_{33}
124.1	0.177	−0.465
93.1	0.123	−0.392
81.5	0.603	−0.698
55.5	0.426	−0.277

Table 12 shows the ion contribution to $Sr_2Ta_2O_7$ piezoelectric components. The greater contribution to e_{31} is from O1, besides O2, and O5. The calculated e_{33} is −2.813 C/m^2, O1, O2, O3, and Sr_2 have a relatively large contribution, with the greatest contribution from O1. In addition, the contribution of ion to dielectric (Table 9) shows that the contribution of ions with large dielectric components to the piezoelectric components are also significant.

Table 12. Contribution of individual ions to the internal-strain piezoelectric constants $e_{iv,\mathrm{int}}$ (in units C/m^2) for $Sr_2Ta_2O_7$.

Atom	WP	$e_{31,\mathrm{int}}$	$e_{33,\mathrm{int}}$
Sr1	4*c*	0.085	–0.113
Sr2	4*c*	0.005	–0.129
Ta1	4*c*	0.090	–0.085
Ta2	4*c*	–0.092	0.183
O1	4*c*	0.324	–0.594
O2	4*c*	0.182	–0.227
O3	8*f*	0.028	–0232
O4	8*f*	0.77	–0.049
O5	4*a*	0.142	–0.115

3.3. The Born effective charge and spontaneous polarization of $Sr_2M_2O_7$

The Born effective charge of $Sr_2Nb_2O_7$ are shown in Table 13, because of symmetry, only Z^k_{xx}, Z^k_{yy}, and Z^k_{zz} are listed. This is similar to the ABO_3 perovskite structure compound,[22] and the Born effective charge of each atom is deviated from the valence, this is particularly evident for the Nb and O in $Sr_2Nb_2O_7$. As seen from the table, the Born effective charge of Nb_1 and Nb_2 along the x axis are 7.864 and 7.788, respectively. Meanwhile, the Born effective charge of O_4 and O_5 are –5.966 and –6.040, which are almost triple as much as O^{-2}. The root reasons are the covalent properties and the hybridization between O-2p and Nb-4d. The Nb–O covalent bond is stronger than the Sr–O ionic bond. It is clear that the Born effective charge of O along the Nb–O is greater than the others. Therefore, the anisotropy is determined by the covalence of Nb–O.

Table 13. The Born effective charge for each inequivalent atom in the $Cmc2_1$ sapce group of the $Sr_2Nb_2O_7$ structure.

Atom	$\overline{Z}^k_{xx}$	$\overline{Z}^k_{yy}$	$\overline{Z}^k_{zz}$
Sr1 (4*a*)	2.611	2.992	2.840
Sr2 (4*a*)	2.608	2.115	2.643
Nb1 (4*a*)	7.864	6.349	6.041
Nb2 (4*a*)	7.788	5.631	7.515
O1 (4*a*)	–1.999	–2.895	–3.454
O2 (4*a*)	–1.366	–2.809	–3.159
O3 (4*a*)	–1.865	–3.088	–2.639
O4 (4*a*)	–5.966	–1.288	–1.711
O5 (4*a*)	–6.040	–1.569	–1.292
O6 (4*a*)	–1.541	–2.259	–2.957
O7 (4*a*)	–1.947	–3.197	–3.833

At room temperature, the spontaneous polarization of $Sr_2Nb_2O_7$ was reported in the direction [001], which is 9 μC/cm^2.[5] According to Berry-phase polarization theory, we calculated the spontaneous polarization of $Sr_2Nb_2O_7$ in the same direction, but 25 μC/cm^2. Because of the temperature, it is reasonable to make a difference in the spontaneous polarization. $Sr_2Ta_2O_7$ has no spontaneous polarization in the paraelectric state.

$Sr_2Nb_2O_7$ is an environmently-friendly piezoelectric material, and due to its high Curie point, it can be applied to high temperature conditions. $PbTiO_3$[27] as one of the earliest discovered piezoelectric materials with good performance, and the piezoelectric constants were $e_{15} = 4.03$ C/m^2, $e_{31} = 1.81$ C/m^2, and $e_{33} = 3.23$ C/m^2, respectively. The piezoelectric properties of $Sr_2Nb_2O_7$ need to be improved by comparison with $PbTiO_3$.[28] It is well known that stress has an effect on improving the physical properties of ferroelectric materials.[29] Therefore, we tried to apply a pressure on $Sr_2Nb_2O_7$, and the pressure was 0–4.5 GPa on the premise that the material did not have structural phase transition.

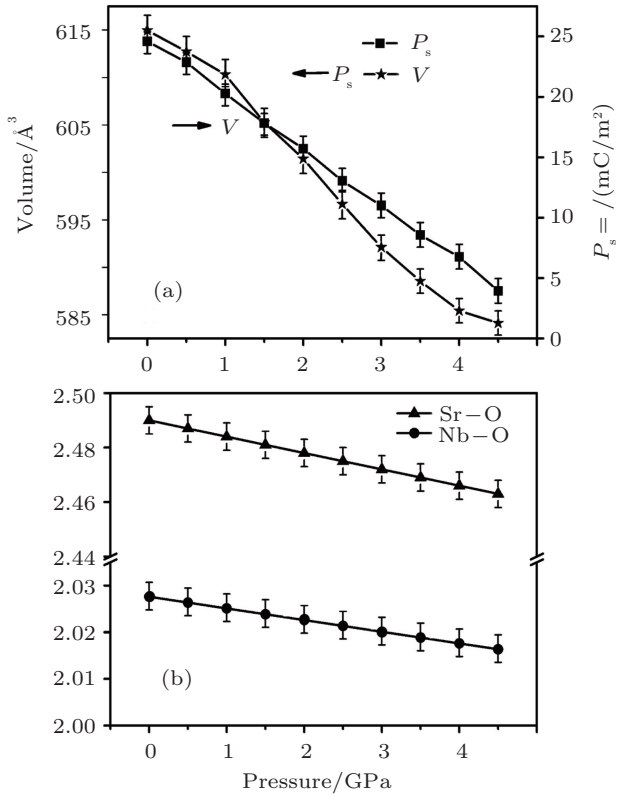


Fig. 4. The charge relation of volume, polarization, and bond length with pressure increase.

The changes of volume V, polarization P_s, and bond length with pressure increases are shown in Fig. 4, and it can be seen that parameters are all decreased in the pressure range. When the pressure reaches 4.5 GPa, the volume reduces to 588.19 Å^3, and the polarization is just 1.34 μC/cm^2. Because the volume decreases and the atomic position changes, the average bond lengths of the Sr–O and Nb–O shorten as well. This can also be attributed to the chain reaction in the crystal lattice along the crystal axis. Moreover, the long-range Coulomb force weakens and the short-range repulsion increases, which will restrain the ferroelectric properties of the material.

The results of further analysis of the relations among pressure, volume, and polarization (Fig. 4(a)) are summarized as follows. Firstly, the volume decreases to 599.23 Å^3 when the pressure increases to about 2.5 GPa, the polarization is about 10 μC/cm^2, which are in good agreement with the experimental values.[30] Therefore, we review the previous polarization results are greater than the experiment, perhaps because of the selection of function and limitations of simulation calculation. What is more, the negative pressure on the material may improve the spontaneous polarization and ferroelectric properties. Finally, in order to increase the tensile stress on the surface, by adding a substrate to $Sr_2Nb_2O_7$ so that lattice constants are slightly greater in the epitaxial-coating can also reach the goal of improving the properties.

4. Conclusion

First-principles calculations have been performed to study $Sr_2M_2O_7$, the optimized structures are consistent with previous experimental and theoretical data, which can indicate that our calculation method is reasonable. By comparing the dielectric constants in the experiment, the calculated results of $Sr_2Nb_2O_7$ and $Sr_2Ta_2O_7$ are within the limits of error. In addition, from the viewpoint of optical modes and phonons, the contribution and influence of the phonon modes at different frequencies and the various ions to the dielectric and piezoelectric properties were analyzed. For $Sr_2Ta_2O_7$, the phonon frequencies were also investigated, but there was no corresponding experimental data to compare with.

The larger values of $Sr_2Nb_2O_7$ piezoelectric components are e_{31} and e_{33}, 1.276 C/m^2 and –2.932 C/m^2, respectively. The contribution to the piezoelectric component mainly comes from the A_1. The spontaneous polarization of $Sr_2Nb_2O_7$ is 25 μC/cm^2 in the direction [001], which is slightly larger than the experimental value. After pressure, the polarization of $Sr_2Nb_2O_7$ decreases linearly with the increasing pressure. Therefore, the application of tensile stress on the surface or negative pressure can enhance the spontaneous polarization and ferroelectric properties of the material.

Throughout the article, the study of lattice vibration is the key point, which relates to the properties of materials such as electromagnetism, specific heat, thermal conductivity, and conductance; our theoretical results will provide a guide to further investigate $Sr_2M_2O_7$.

References

[1] Cai X, Teng Y, Wu L and Zhang K 2016 *J. Mater. Sci.-Mater. Electron.* **28** 4239
[2] Chen T, Liang R H, Jiang K, Hu Z G, Zhou Z Y and Dong X L 2017 *J. Am. Ceram. Soc.* **100** 2397
[3] Peng Y, Ma Z, Hu J and Wu K 2017 *RSC Adv.* **7** 40922
[4] Teshima K, Hara Y, Yubuta K, Oishi S, Domen D and Hojamberdiev M 2017 *Cryst. Growth Des.* **17** 1583
[5] Chen G, Gong C W, Fu C L, Peng X D, Cai W and Gao R L 2015 *Mater. Sci. Forum.* **815** 125
[6] Liou Y C, Tsai W C, Yu J Y and Tsai H C 2015 *Ceram. Int.* **41** 7036
[7] Kudo A, Kato H and Nakagawa S 2000 *J. Phys. Chem. B* **104** 571
[8] Sun L, Wu W, Tian Q, Lei M, Dai Z and Xiao X 2016 *Mater. Sci. Semicond. Process.* **41** 411

[9] Nanamatsu S, Kimura M and Kawamura T 1975 *J. Phys. Soc. Jpn.* **38** 817
[10] Kudo A and Kato H 2001 *J. Photochem. Photobiol. A* **145** 129
[11] Kato K 2000 *J. Mater. Sci.-Mater. Electron.* **11** 575
[12] Yoshioka K, Petrykin V, Kakihana M, Kato H and Kudo A 2005 *J. Catal.* **232** 102
[13] Huang H M, Jiang Z Y and Luo S J 2017 *Chin. Phys. B* **26** 096301
[14] Ma Z N, Quan Z, Wang Q J, Wang X and Wang L 2016 *Acta Phys. Sin.* **65** 236101 (in Chinese)
[15] Shao K, Han H, Zhang W, Wang C Y, Guo Y L, Ren C L and Huai P 2017 *Chin. Phys. B* **26** 097101
[16] Nisar J, Pathak B and Ahuja R 2012 *Appl. Phys. Lett.* **100** 81903
[17] Liu P, Nisar J, Ahuja R and Pathak B 2013 *J. Phys. Chem. C* **117** 13845
[18] Perdew J P, Burke K and Ernzerhof M 1996 *Phys. Rev. Lett.* **77** 3865
[19] Clark S J, Segall M D, Pickard C J, Hasnip P J, Probert M I J and Refson K 2005 *Z. Kristallogr.* **220** 567
[20] Malik R, Franke L and Siebes A 2001 *Thin Solid Films* **381** 176
[21] Baroni S, De Gironcoli S, Dal Corso A and Giannozzi P 2001 *Rev. Mod. Phys.* **73** 515
[22] Di X 2009 *Rev. Mod. Phys.* **82** 1959
[23] Ito K, Horikoshi T and Ohi K 1997 *Ferroelectrics* **203** 201
[24] Liu X Q and Chen X M 2002 *Ceram. Int.* **28** 209
[25] Hushur A and Kojima S 2006 *Mater. Sci. Eng. A* **442** 35
[26] Ning H, Yan H and Reece M J 2010 *J. Am. Ceram. Soc.* **93** 1409
[27] Zhu Z Y, Wang S Q and Fu Y M 2016 *Chin. Phys. Lett.* **33** 026302
[28] De G S, Baroni S and Resta R 1989 *Phys. Rev. Lett.* **62** 2853
[29] Akishige Y, Kamata M and Tsukada S 2015 *Ferroelectrics* **485** 73
[30] Eglitis R I and Vanderbilt D 2007 *Phys. Rev. B* **76** 155436